Selective antibacterial activity and lipid membrane interactions of arginine-rich amphiphilic peptides

ACS APPLIED BIO MATERIALS

www.acsabm.org Article

Selective Antibacterial Activity and Lipid Membrane Interactions of Arginine-Rich Amphiphilic Peptides

Charlotte J. C. Edwards-Gayle, Glyn Barrett, Shyamali Roy, Valeria Castelletto, Jani Seitsonen, Janne Ruokolainen, and Ian W. Hamley*

Cite This: https://dx.doi.org/10.1021/acsabm.9b00894 Read Online

ACCESS | Metrics & More | Article Recommendations | Supporting Information

ABSTRACT: The self-assembly behavior and antimicrobial activity of two designed amphiphilic peptides, R_3F_3 and R_4F_4, containing short hydrophobic phenylalanine (F) and cationic arginine (R) sequences, are investigated. The conformation of the peptides was examined using circular dichroism and FTIR spectroscopy, which show that they have a disordered secondary structure. Concentration-dependent fluorescence assays show the presence of a critical aggregation concentration (cac) for each peptide. Above the cac, small-angle X-ray scattering (SAXS) and transmission electron microscopy (TEM) reveal a population of twisted tapes for R_3F_3 and nanosheets for R_4F_4. The interaction of the peptides with model bacterial membranes comprising mixtures of the lipids DPPG [1,2-dipalmitoyl-*sn*-glycero-3-phosphoglycerol] and DPPE [1,2-dipalmitoyl-*sn*-glycero-3-phosphoethanolamine], was studied using SAXS and cryogenic-TEM. Analysis of the SAXS structure factor indicates that R_3F_3 interacts with lipid bilayers by inducing correlation between bilayers, whereas R_4F_4 interacts with the bilayers causing an increase in polydispersity of the vesicle wall thickness. Both peptides break vesicles with a 1:3 DPPG:DPPE composition, which is close to the ratio of PG and PE lipids observed in the lipid membrane of *Pseudomonas aeruginosa*, a pathogen responsible for serious infections and which has developed antimicrobial resistant strains. Both peptides show activity against this bacterium in planktonic form. Peptide R_4F_4 shows particularly strong bioactivity against this microbe, with a minimum inhibitory concentration (MIC) value in the range of concentrations where the peptide is cytocompatible. It was further shown to have activity against other *Pseudomonas* species including the common plant pathogen *Pseudomonas syringae*. Finally, we show that R_4F_4 inhibits the development of *P. aeruginosa* biofilms. This was examined in detail and a proposed mechanism involving binding of the signaling molecule c-di-GMP is suggested, based on circular dichroism spectroscopy studies and Congo red assays of extracellular polysaccharides produced by the stressed bacteria. Thus, R_4F_4 is a promising candidate antimicrobial peptide with activity against *Pseudomonas* species.

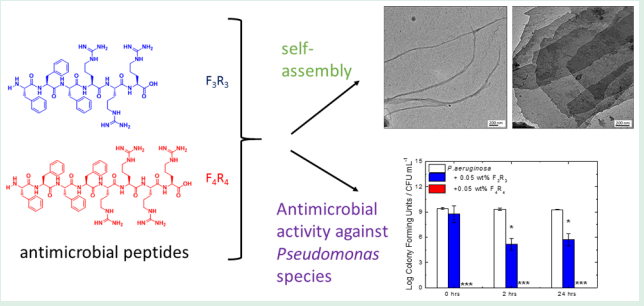

KEYWORDS: *peptide, liposomes, model membranes, antimicrobial, self-assembly, SAXS*

INTRODUCTION

The increase in prevalence of multi-antibiotic-resistant pathogens is of great concern and has been listed by the World Health Organization (WHO) as one of the biggest threats to modern day healthcare, food security, and development. There is great interest in the development of new therapeutics to overcome this. Peptides, especially those containing cationic residues or tryptophan, have been shown to have great potential in this regard.[1,2] Many antimicrobial peptides have evolved naturally in species of plants and animals, providing a strong basis to produce biocompatible therapeutics. Peptides with the ability to self-assemble are of interest as they may have increased in vivo stability through increased half-life and resistance to proteolysis.

Antimicrobial peptides are thought to interact with the cell membranes of bacteria through different mechanisms.[2] It has been proposed that some peptides induce pore formation where the pore is lined with peptide (the barrel-stave model), or when the peptide causes curvature of the lipid membrane (the toroidal pore model).[3] Another mechanism involves peptide deposition on the membrane surface (the carpet model), which is followed by a detergent-like action that leads to pore formation.[3] Cationic peptides are able to associate with the membrane and cause an electrical potential difference across the membrane, inducing electroporation (the molecular electroporation model).[4]

Received: November 26, 2019
Accepted: January 21, 2020
Published: January 21, 2020

An important class of antimicrobial peptide are those containing L-arginine.[2] L-Arginine is commonly found as an active site residue in proteins and is common in many cell-penetrating peptides. The antimicrobial activity of L-arginine is due to the cationic charge of this amino acid which interacts with anionic or zwitterionic lipid membranes, which may lead to pore formation.[5,6]

Surfactant-like peptides (SLPs) are a group of peptides with promising applications as antimicrobials. Structurally, SLPs have a headgroup of a small sequence of charged residues and a longer hydrophobic tail, which gives them remarkable self-assembling properties.[7−9] Recently, the self-assembly of three SLPs, A_3K, A_6K, and A_9K, was examined and distinct morphologies were observed for the three peptides.[10] The antimicrobial properties were found to be dependent on the length of the hydrophobic chain, with A_9K being most active against *Escherichia coli* and *Staphylococcus aureus*, also strongly disrupting the structure of anionic vesicle DPPG,[10] used as a model system for bacterial cell membranes.

Our group has studied the self-assembly properties and antimicrobial activities of several SLPs containing one or two arginine residues. Surfactant-like peptide A_6R was found to self-assemble into nanofibers, and to have antimicrobial activity.[11,12] More recently, A_6R in both capped and uncapped forms was examined. CapA_6R forms nanofibrils, whereas A_6R assembles into nanotapes, which preferentially interacted with lipid POPG in POPG/POPE vesicles [POPG = 2-oleoyl-1-palmitoyl-*sn*-glycero-3-phosphoglycerol, POPE = 2-oleoyl-1-palmitoyl-*sn*-glycero-3-phosphoethanolamine].[13] The capped A_6R variant showed selective activity against Gram-positive *Listeria monocytogenes*, and the uncapped version showed greater antimicrobial activity against this and also *E. coli* and *S. aureus*.[13] Another surfactant-like peptide, RA_3R, containing arginine on both termini, was found to assemble into a polyproline II helix in water, which interacted strongly with POPG in mixed lipid vesicles.[14] RA_3R was found to be particularly active against *L. monocytogenes* through membrane reorganization.

Here, we examine the self-assembly behavior and antimicrobial activity of two SLPs with sequences RRRFFF (R_3F_3) and RRRRFFFF (R_4F_4) (Scheme 1). These peptides comprise a hydrophobic phenylalanine block and a block of cationic L-arginine residues, and were designed as novel arginine-rich SLPs containing aromatic hydrophobic blocks, incorporated to drive self-assembly via π-stacking interactions. Recently, Silva et al. examined the self-assembly of peptides consisting of alternating RF motifs. The short oligopeptide $[RF]_4$ was found to assemble into highly ordered amyloid-like fibrils above a critical aggregation concentration.[15] Further studies of $[RF]_n$, where n is between 1 and 5, showed an increased structural order and cytotoxicity with increasing n.[16] In another example, Fojan et al. studied the self-assembly of RFFFR, which was shown to self-assemble into fibers stabilized by π-stacking interactions, which further assembled into solid spheres.[17]

The two peptides we investigate, R_3F_3 and R_4F_4, are architecturally different from these previously studied RF-containing peptides and surfactant-like peptides, as they contain blocks of symmetric charged and hydrophobic blocks.

We first present results on the self-assembly and conformation of R_3F_3 and R_4F_4. We, then, examine the interactions of these peptides with DPPG/DPPE vesicles. DPPG (1,2-dipalmitoyl-*sn*-glycero-3-phosphoglycerol), is anionic, whereas DPPE (1,2-dipalmyitoyl-*sn*-glycero-3-phosphoethanolamine) is zwitterionic. Cationic peptides have the ability to distinguish between human cell membranes, which mainly contain lipids based on phosphocholine (PC), as opposed to bacterial cell membranes, which contain significant quantities of PG (phosphoglyercol) and PE (phosphoethanolamine) lipids.[13,14,18,19] Examining the interactions of the two peptides with these bacterial membrane models enables greater understanding of the mechanisms by which these peptides interact with specific membrane constituents of bacteria. Typically, more PG lipids are found in Gram-positive bacteria, whereas PE lipids are generally more abundant in Gram-negative bacteria.[20] We study the interaction of the two designed peptides with model lipid membranes with different ratios of PG/PE, to better understand antimicrobial activity. Specifically, we examine the interactions of the peptides with mixed lipids comprising ratios PG/PE and 3:1, 1:1, 1:3, and 1:0, in line with a previous study.[19] The combination of DPPG and DPPE was chosen due to the accessible melting temperature T_m values, which are well separated for the two lipids, being reported to be 41 and 63 °C, respectively.[21]

Finally, we examine the antibacterial activity of these peptides against four species of bacteria, *E. coli*, *S. aureus*, *Pseudomonas aeruginosa*, and *Pseudomonas syringae*. Since minimal toxicity to human cells is an essential requirement of an effective peptide therapeutic, we also assay the cytocompatibility of these peptides using a human skin fibroblast model.

Scheme 1. Structures of Peptides RRRFFF (R_3F_3), RRRRFFFF (R_4F_4), and the Two Lipids Used in Model Membranes, 1,2-dipalmitoyl-*sn*-glycero-3-phosphoglycerol (DPPG) and 1,2-dipalmitoyl-*sn*-glycero-3-phosphoethanolamine (DPPE)

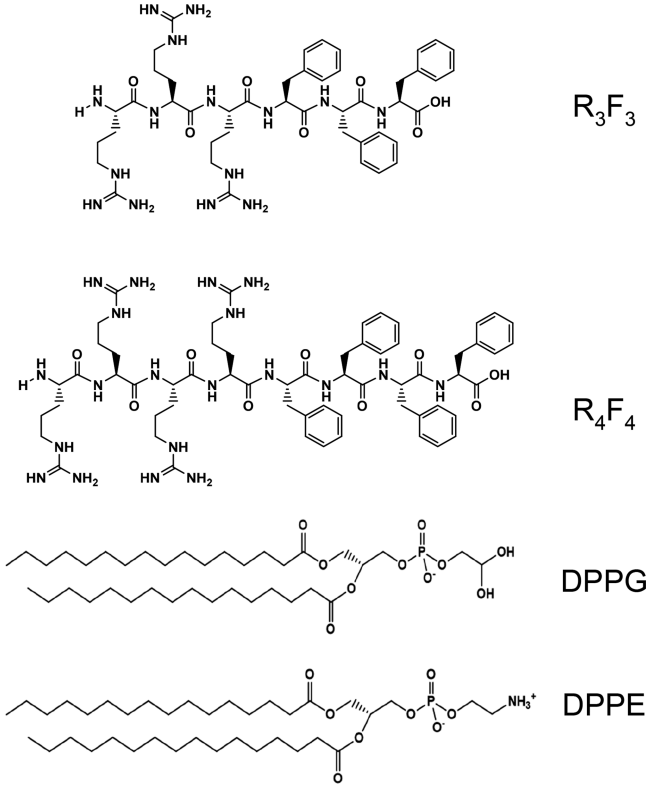

https://dx.doi.org/10.1021/acsabm.9b00894
ACS Appl. Bio Mater. XXXX, XXX, XXX−XXX

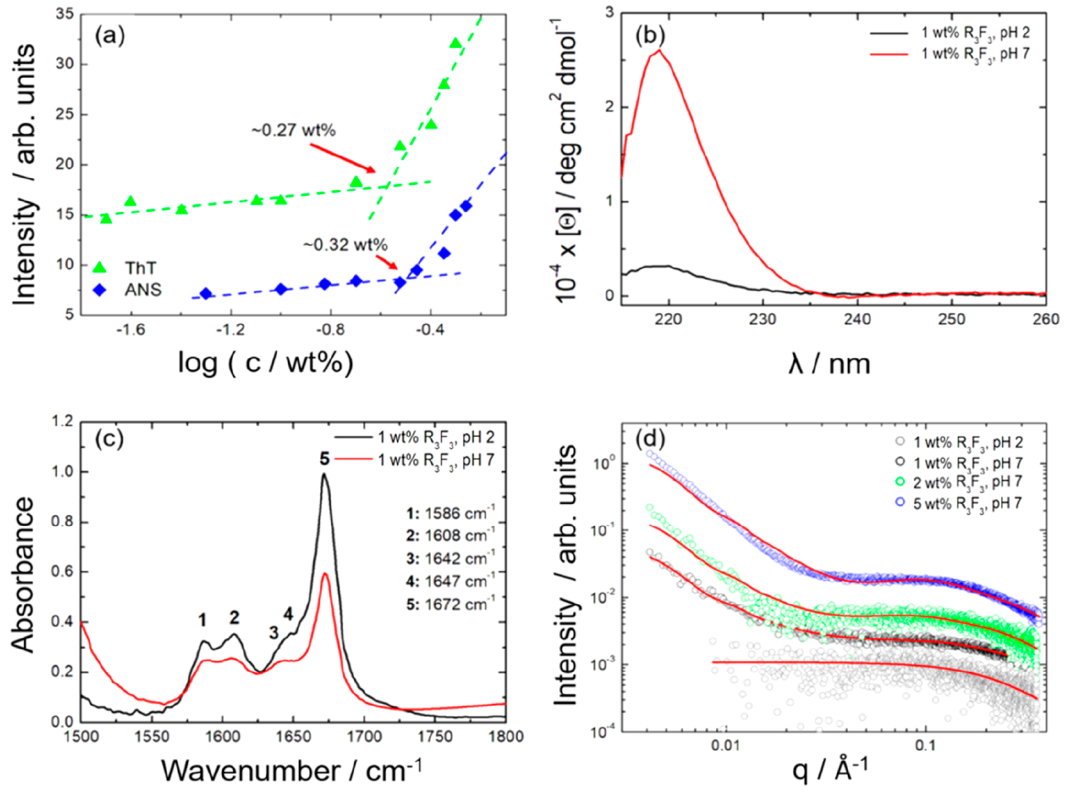

Figure 1. Conformation and self-assembly of R_3F_3: (a) fluorescence assay to determined cac using ANS and ThT at native pH (pH 2), (b) CD spectra at pH values indicated, (c) FTIR spectra at pH values indicated, and (d) SAXS data with fitted form factors in red.

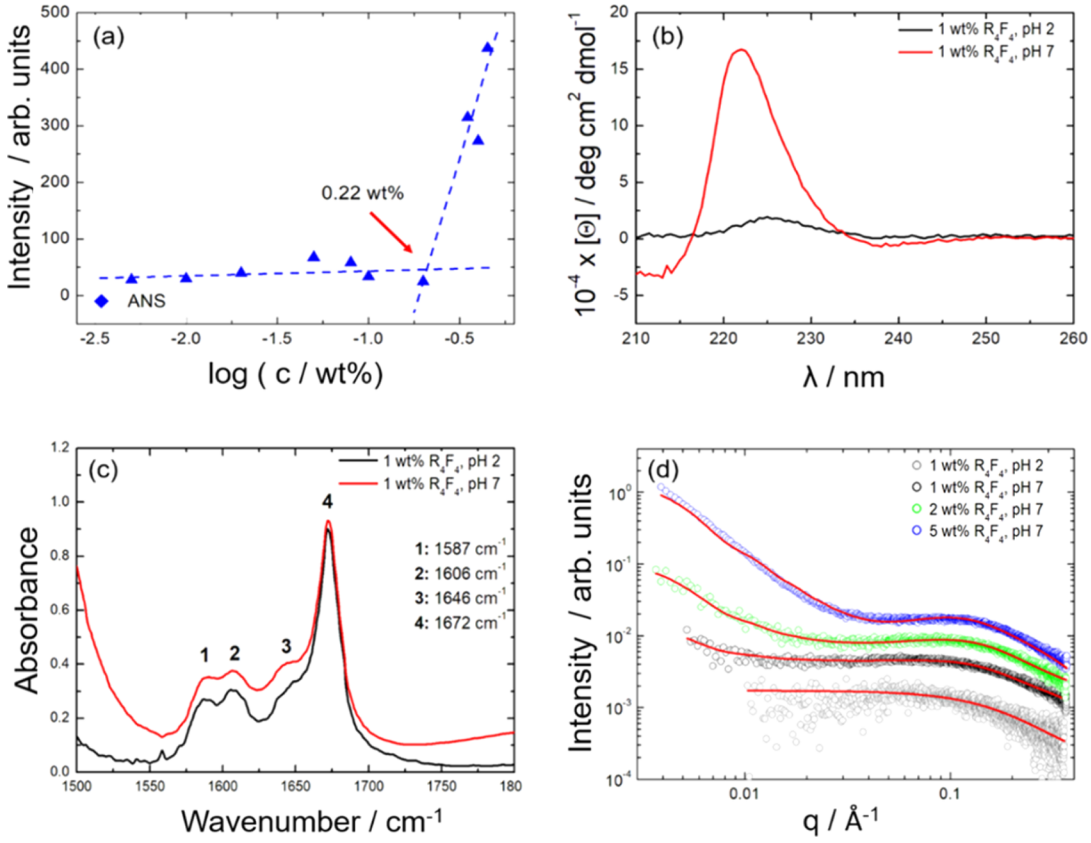

Figure 2. Conformation and self-assembly of R_4F_4: (a) fluorescence assay to determine cac using ANS at native pH (pH 2), (b) CD spectra at pH values indicated, (c) FTIR spectra at pH values indicated, and (d) SAXS data with fitted form factors in red.

https://dx.doi.org/10.1021/acsabm.9b00894
ACS Appl. Bio Mater. XXXX, XXX, XXX−XXX

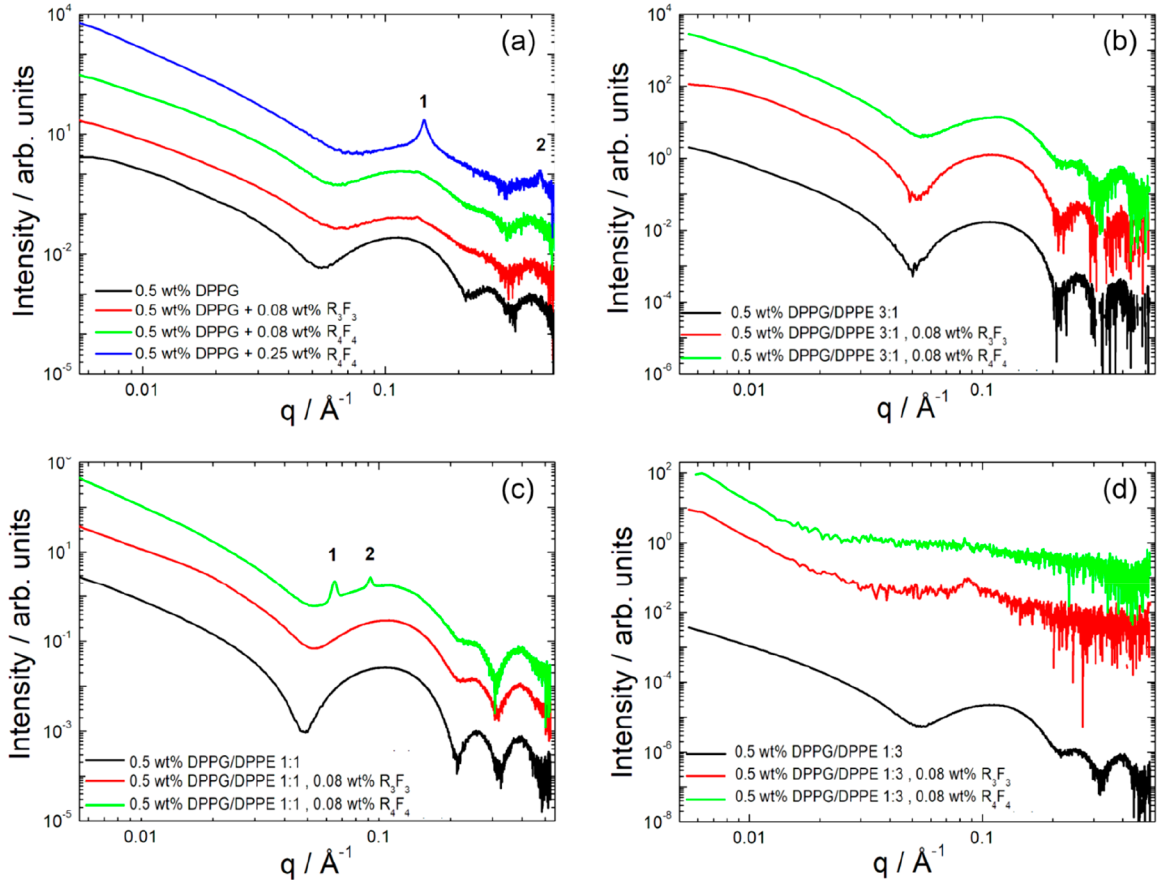

Figure 3. SAXS profiles for different liposome compositions (expressed in terms of ratios of DPPG/DPPE) in the presence of R_3F_3 or R_4F_4 at the concentrations indicated: (a) DPPG vesicles alone, (b) DPPG/DPPE 3:1, (c) DPPG/DPPE 1:1, and (d) DPPG/DPPE 1:3. Bragg peaks are numbered.

RESULTS

Self-Assembly. The critical aggregation concentration (cac) for both R_3F_3 and R_4F_4 was determined using 8-anilinonaphthalene-1-sulfonic acid (ANS), which is used because its fluorescence changes within a hydrophobic environment. The cac values for R_3F_3 (Figure 1a) and R_4F_4 (Figure 2a) were found to be (0.32 ± 0.02) and (0.22 ± 0.03) wt % respectively. There is a significant difference in cac values, the cac being lower for R_4F_4 than for R_3F_3, which suggests that the cac depends not just on the balance of hydrophobic and charged residues but is also influenced by the number of charged residues. To further assess the critical aggregation concentration, the amyloid-sensitive fluorophore thioflavin T (ThT) was used. Only R_3F_3 was found to bind significantly to ThT, indicating that it forms amyloid-like fibers. As shown in Figure 1a, the cac of R_3F_3 determined by ThT fluorescence assays was found to be (0.27 ± 0.03) wt %, which is consistent within uncertainty with that detected by ANS. This suggests that hydrophobic collapse occurs at the same concentration as the formation of amyloid structures by R_3F_3.

To examine the secondary structure of R_3F_3 and R_4F_4, circular dichroism and Fourier transform infrared spectroscopy were conducted above the cac. The CD spectra are dominated by electronic transitions associated with the phenylalanine side chain. The main feature (Figures 1b and 2b) for all spectra is the peak at 220 nm which is due to phenylalanine π-stacking electronic transitions.[22] The molar ellipticity increases when the pH of solutions of R_3F_3 and R_4F_4 was adjusted to pH 7. This indicates an increase in content of chiral structures. FTIR (Figures 1c and 2c) was used to further probe secondary structure. The data shows a peak at 1673 cm^{-1}, which can be assigned to vibrations of the TFA counterions bound to the peptide.[23] The peak at 1645 cm^{-1}, characteristic of a disordered secondary structure, is present only at native pH for both peptides. All spectra show a peak at 1608 cm^{-1}, which is characteristic of arginine side chains.[23,24] The peak at 1588 cm^{-1} can be assigned to the arginine side chain guanidinium group symmetric stretch. The 1456 cm^{-1} peak can be ascribed to $-CH_2$ bond vibrations.[25] Considering the data from both CD and FTIR spectroscopy, we conclude that at native pH, R_3F_3, and R_4F_4 have a disordered secondary structure.

TEM was used to image the self-assembled structure of R_3F_3 and R_4F_4 (Figure S1). Self-assembled structures were observed for both peptides, with R_3F_3 forming a population of twisted nanotapes, that are several microns long, with a width between 50 and 120 nm. The presence of nanotapes agrees with the binding of fluorescent probe ThT. R_4F_4 was found to assemble into a population of large nanosheets of differing sizes with widths between 342 and 1.7 μm. These non-amyloid structures are not expected to bind ThT, consistent with the fluorescence binding assays.

To further probe the self-assembled structures, SAXS measurements were performed (Figures 1d and 2d) in dilute solutions to provide form factors. These are analyzed to provide information on the shape and dimensions of self-assembled nanostructures. Data from peptide solutions at pH 7

https://dx.doi.org/10.1021/acsabm.9b00894
ACS Appl. Bio Mater. XXXX, XXX, XXX−XXX

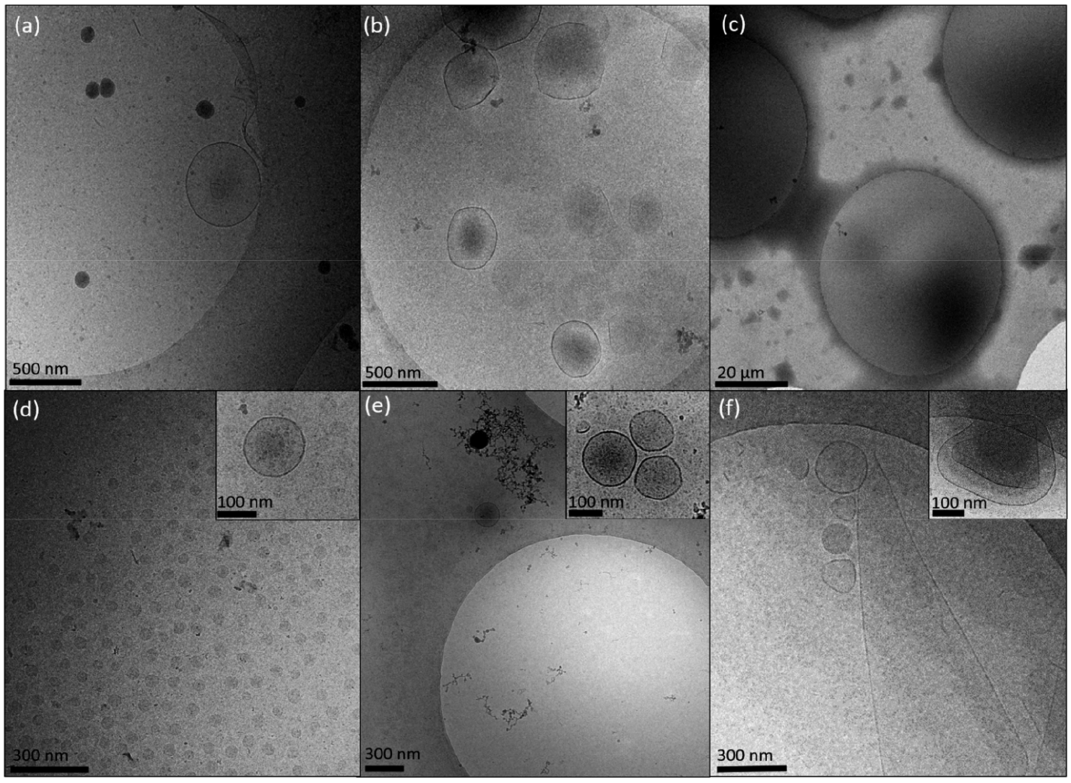

Figure 4. Cryo-TEM images of vesicles with and without peptide: (a) 0.5 wt % DPPG/DPPE 1:3, (b) 0.5 wt % DPPG/DPPE 1:3 + 0.08 wt % R_3F_3, (c) 0.5 wt % DPPG/DPPE 1:3 + 0.08 wt % R_4F_4, (d) 0.5 wt % DPPG, (e) 0.5 wt % DPPG + 0.08 wt % R_3F_3, and (f) 0.5 wt % DPPG + 0.08 wt % R_4F_4.

show initial intensity decays with q^{-2} which indicates planar structures. The data was fitted to a bilayer Gaussian form factor model (previously used by our group to describe the density profile across a bilayer),[23,26] and a generalized Gaussian coil form factor to account for any monomers remaining in the solution (Tables S1 and S2) using the software SASfit.[27] This model fits the data very well. An estimate of the length of the peptide (assuming an antiparallel β-sheet structure) is the number of residues multiplied by 3.4 Å.[28] The approximate length of R_3F_3 and R_4F_4 is 20 and 27 Å, respectively. The bilayer thickness obtained from the SAXS fits corresponds approximately to these values implying that the nanosheets and twisted tapes are one molecule thick. This suggests an antiparallel arrangement leading to arginine-coated nanotapes/nanosheets (a nanosheet structure with this configuration was proposed for A_6R).[12] From these measurements, we conclude that the peptides form a small population of bilayer structures, with a larger population of unaggregated peptides. Adjustment to pH 7 increases the population of these structures.

Interaction with Lipid Vesicles. To understand the antimicrobial activity of R_3F_3 and R_4F_4 discussed in the following section, which is due to interaction of the arginine residues with lipid headgroups, we examined whether there were any interactions between the peptides and the model DPPG/DPPE liposomes, a system commonly used as a bacterial membrane model.[10,19] SAXS was used to probe structure changes resulting from interaction of peptides with lipid membranes. We examined the ratios 1:0, 1:3, 1:1, and 3:1 of DPPG/DPPE. In accordance with the phase diagrams recorded previously,[19] the samples with mixtures 1:0, 1:1, and 3:1 DPPG/DPPE are expected to be in the disordered liquid crystal (L_α) phase at 20 °C, whereas 1:3 DPPG/DPPE is expected to be in the L_α/L_β coexistence region at 20 °C (where L_β is the ordered gel phase). PE alone is not studied because of the shape of the lipid it forms inverted micelles with hexagonal symmetry.[14]

Figure 3 shows SAXS intensity profiles obtained with ratios 1:0, 1:3, 1:1, and 3:1 of DPPG/DPPE at 0.5 wt % with and without R_3F_3 and R_4F_4. For all ratios, the SAXS patterns for the liposomes of lipids alone displayed a broad scattering peak centered at $q \sim 0.1$ Å^{-1}, which is associated with unilamellar vesicles.[13] Figure 3 also contains the SAXS data for samples with added peptide. A concentration of 0.08 wt % peptide was used (data being shown for an additional concentration of 0.25 wt % for R_4F_4 with DPPG), since addition of 0.25 wt % peptide caused precipitation in many samples, as seen with previously studied peptides.[13,14]

In the SAXS data for 1:0 DPPG/DPPE, 0.08 wt % R_3F_3, there is a small Bragg peak, with a corresponding domain spacing d = 45.9 Å and a distortion of the broad peak shape. This indicates some correlation between bilayers, that is, restructuring of a proportion of vesicles into multilamellar vesicles. Adding 0.08 wt % R_4F_4 to DPPG leads to a change in the shape of the SAXS profile (broadening of the form factor extrema), and when the concentration of R_4F_4 is increased to 0.25 wt %, two Bragg peaks with d = 43.4 and 14.6 Å are present. These peaks correspond to the first- and third-order reflections of a multilamellar structure, indicating that restructuring of most liposomes into multilamellar vesicles occurs in the presence of R_4F_4 at this concentration, indicating peptide-induced lipid restructuring. R_3F_3 was not examined at this concentration due to precipitation of the sample.

https://dx.doi.org/10.1021/acsabm.9b00894
ACS Appl. Bio Mater. XXXX, XXX, XXX−XXX

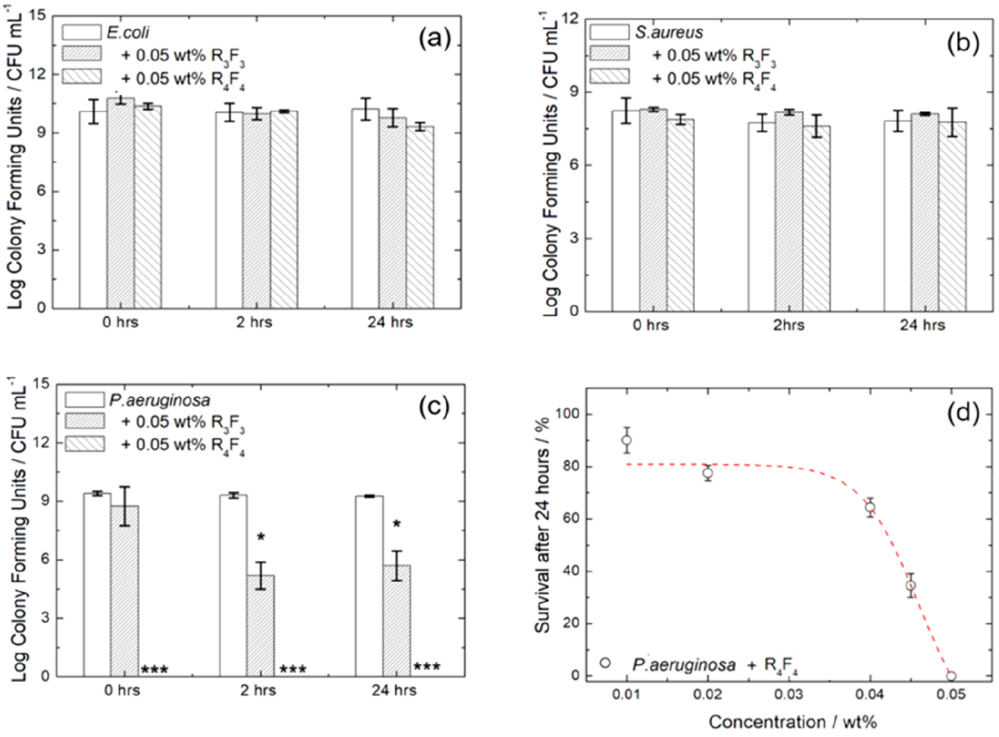

Figure 5. Activity of R_3F_3 and R_4F_4 against several strains of bacteria, (a) *E. coli*, (b) *S. aureus*, and (c) *P. aeruginosa*, and (d) MIC determination for R_4F_4 with *P. aeruginosa*. *= $p < 0.05$, ** = $p < 0.01$, and ***$p < 0.001$.

For the lipid mixture 3:1 DPPG/DPPE, no Bragg peak was observed in the SAXS profiles in the presence of either peptide, indeed the form factor resembles that for the corresponding mixed liposome, with again only some broadening of form factor features (and a shift to higher q) particularly in the presence of R_4F_4. For R_3F_3 combined with 1:1 DPPG:DPPE, there is again a broadening in the features in the SAXS curve. However, for R_4F_4, two Bragg peaks are noted with corresponding spacings d = 96.0 and 68.2 Å, which is approximately a 1: $\sqrt{2}$ ratio suggesting cubic symmetry, although the presence of two coexisting lamellar structures cannot be excluded in the absence of higher order Bragg reflections. This feature is not observed for R_3F_3.

Considering the SAXS data for the samples containing most DPPE (1:3 DPPG/DPPE), the liposome form factor is lost upon addition of either peptide, this being replaced with form factor profiles with a shape dominated at low q by scattering from the peptides alone (Figures 1d and 2d), especially for R_4F_4, although there is a Bragg peak for R_3F_3, showing some multilamellar vesicles are still present. Cryo-TEM images of samples prepared with lipids at this ratio show that R_3F_3 causes a change in morphology of liposomes, seen by the appearance of rougher looking surfaces (Figure 4b). Cryo-TEM images of samples with this lipid composition in the presence of R_4F_4 show that the peptide induces complete disruption of liposome formation, in agreement with conclusions from the SAXS data (Figure 4c). The Cryo-TEM image for vesicles of DPPG (Figure 4d) shows that vesicles are generally larger when exposed to R_3F_3 with some fibers (presumably peptide) also present (Figure 4e), whereas with R_4F_4, the vesicles are more swollen and, moreover, are much more angular in shape and have a multilamellar structure (Figure 4f). This is consistent with the SAXS data shown in Figure 3a.

Circular dichroism spectroscopy is often also used to examine the interactions of lipid membranes with peptides.[13,14,29] In some instances, peptide secondary structure is shown to be influenced in the presence of lipid membranes which can induce the formation of more ordered secondary structure. This moreover gives information about whether the peptide interacts with the lipid as a monomer or as a self-assembled structure. Figure S2 shows the circular dichroism spectra for the mixtures of the two peptides with different composition lipid mixtures. Because of presence of the broad maximum around 220 nm in the spectra, it is concluded that the peptides interact with the lipids in a monomeric form.

Before investigating the potential antimicrobial activity of R_3F_3 and R_4F_4, it is desirable to assay cytocompatibility, to determine the concentration range of peptides over which viability of human cells is retained. We therefore performed cytotoxicity assessments using the MTT assay on 161br human skin fibroblasts (Figure S3). The IC_{50} of R_4F_4 was calculated to be 2.15 mM (or 2.64 mg/mL or 0.264 wt %). Interestingly, this is in the error range of the cac value determined for R_4F_4 (Figure 1a) implying that the self-assembly into nanosheet structures correlates to the onset of increased toxicity. The IC_{50} of R_4F_4 is higher than the previously studied $[RF]_4$ peptide, which has an IC_{50} value of less than 1 mM, meaning that R_4F_4 is less cytotoxic. Clearly, sequence has a significant effect on the cytotoxicity of these compositionally identical peptides. The IC_{50} of R_3F_3 was found to be 4.31 mM (4 mg/mL or 0.4 wt %), the maximum concentration used in the concentration series and above the cac of this peptide. The finding that an increased number of residues leads to increased toxicity agrees with studies conducted with $[RF]_n$ repeating peptides,[16] although R_4F_4 is significantly less cytotoxic than its compositional homologue RFRFRFRF.

https://dx.doi.org/10.1021/acsabm.9b00894
ACS Appl. Bio Mater. XXXX, XXX, XXX−XXX

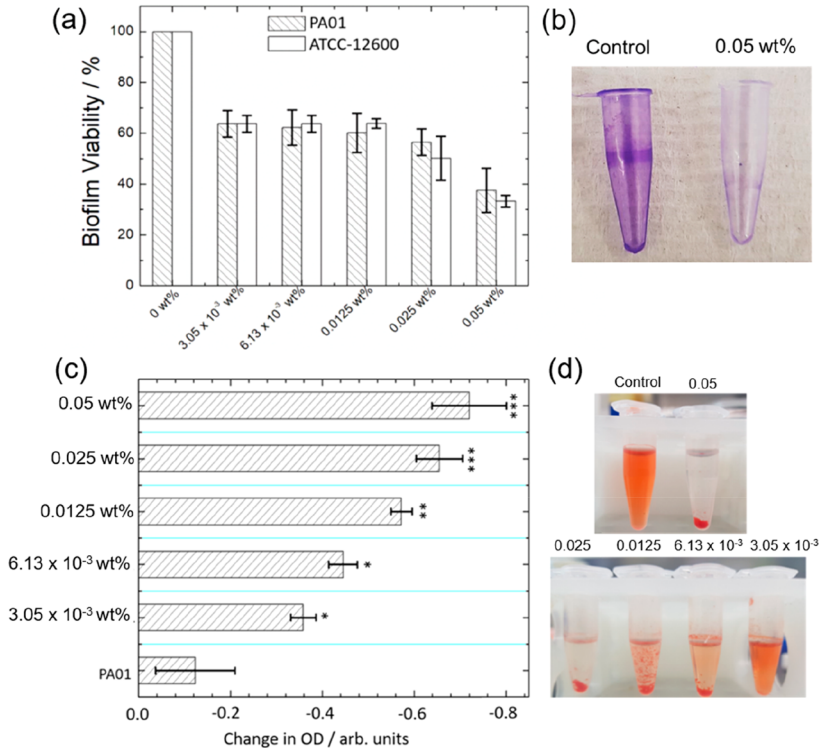

Figure 6. Biofilm assay results: (a) Effect of peptides on biofilm formation after 18 h using a crystal violet assay, (b) images of vials showing crystal violet stain left by biofilms at the air−water interface, after removal of the aqueous phase, (c) Congo red assay, measuring amount of polysaccharide produced by bacteria, at the peptide concentrations indicated, and (d) Congo red staining vials, showing flocculation of the bacteria at the bottom of the tube as opposed to the sides where there is growth.

Having determined conditions where viability of human fibroblasts in the presence of these peptides is acceptable, we then studied their antimicrobial activity. Compounds that are active against bacteria have either inhibitory or bactericidal properties.[30] Inhibitory compounds are less likely to cause bacterial resistance but are more susceptible to the innate immune system and antibiotics. Bactericidal compounds are useful for fighting bacterial infections but can increase the resistance of bacteria. Both activities are valuable for different purposes. To examine whether R_3F_3 and R_4F_4 are bactericidal, the two peptides were inoculated with several strains of bacteria for 24 h. Figure 5 shows the antimicrobial activity of these peptides against Gram-positive *S. aureus* and two Gram-negative bacteria, one strain of *P. aeruginosa* (PA01) and one of *E. coli* (K12). A concentration of 0.05 wt % was selected, based upon the viability of human skin fibroblasts at this concentration, which was shown to be 77% and 81% for R_3F_3 and R_4F_4, respectively (Figure S3). The antimicrobial activity data indicate that R_3F_3 shows no effect on any of these bacteria; however, R_4F_4 causes a small, not statistically significant, reduction of 1 order of magnitude in colony forming units/milliliter (CFU/mL) of *E. coli* (K12) after 24 h. This effect, however, is not seen for the clinically relevant *E. coli* (0157) strain (Figure S4). Both peptides showed no activity against *S. aureus*, in contrast to previously studied arginine-rich peptides,[11,14] although this could be due to the lower concentrations used. Interestingly, both peptides showed a strong antimicrobial effect against *P. aeruginosa* (Figure 5c), with a 3.2 log reduction in CFU/mL upon addition of R_3F_3, and complete death of the strain after 2 h on exposure to 0.05 wt % R_4F_4 (Figure 5c). To investigate this further, a series of concentrations of R_3F_3 (Figure S5) and R_4F_4 (Figure 5d) were examined to locate any MIC. The data indicate that R_3F_3 does not have an MIC below 0.1 wt %, and R_4F_4 has a MIC value between 0.045 and 0.05 wt % for *P. aeruginosa*.

To further understand the specificity of these peptides against *Pseudomonas* bacteria, the antibacterial activity of the peptides against four other species was examined (Figure S6). Since R_4F_4 is particularly active against *Pseudomonas* species, data were obtained for an additional three species. Data for *Pseudomonas putida*, *Pseudomonas agarici*, and *Pseudomonas fluorescens* are shown in Figure S6a−c, and this shows that all bacteria displayed an initial die off when exposed to R_4F_4, but interestingly, *P. fluorescens* shows some recovery in bacterial colony counts after 24 h, perhaps because the bacteria are able to metabolize the peptide, however further studies would be needed to understand this effect. There is also a significant (log 2.6) reduction in CFU/mL of plant pathogen *P. syringae* when exposed to R_3F_3 and a complete bacterial kill when exposed to R_4F_4, similar to the effects seen with *P. aeruginosa* after 2 h of exposure. The MIC concentration is ∼0.001 wt % for *P. syringae*, which is approximately 50× lower than that for *P. aeruginosa*. Our data suggests that R_4F_4 is selectively active against specific *Pseudomonas* species.

Finally, we examined whether our peptides can prevent biofilm formation of *P. aeruginosa*, which is a major problem in infections, in particular those of the respiratory tract. An important regulator of biofilm formation in *P. aeruginosa* is the second messenger signaling molecule bis(3′5′)-cyclic dimeric guanosine monophosphate (c-di-GMP).[31−33] High levels of c-di-GMP in *P. aeruginosa* are associated with the formation of biofilms, which leads to virulence and persistence of bacteria in hosts. Compounds that can reduce and prevent biofilm formation by targeting c-di-GMP are, therefore, attracting

https://dx.doi.org/10.1021/acsabm.9b00894
ACS Appl. Bio Mater. XXXX, XXX, XXX−XXX

attention. We first examined whether R_3F_3 and R_4F_4 inhibit biofilm growth formation and then examined interactions of these peptides with c-di-GMP. Crystal violet was used to assay biofilm formation, this cationic dye binding to anionic polysaccharides in the biofilm.[34] The assay results (Figure 6a) show that R_4F_4 causes a reduction of biofilm formation in two strains of *P. aeruginosa*, PA01 and ATCC-12600. At a concentration 0.05 wt % of R_3F_3, we observe 84% survivability of biofilm (Figure S7), whereas R_4F_4 significantly reduces biofilm viability to 37% of *P. aeruginosa strain* PA01 and 33% for strain ATCC-12600 (Figure 6a). Figure 6b shows images of vials showing the Crystal violet taken up by biofilms formed at the air−water interface, after removal of the aqueous phase. The residual purple coloration of the vial surfaces is due to dye taken up by bacteria in planktonic form.

We used a series of biophysical techniques to observe the interaction of both peptides with ci-d-GMP, including SAXS, CD, and TEM. At concentrations of 100 μM or more, c-di-GMP exists in equilibrium with its homodimer.[33] Interestingly, the CD spectra of R_4F_4 and R_3F_3 show that c-di-GMP causes a strong increase in molar ellipticity (Figure S8a) at a 255 nm maximum for R_3F_3 and a slight red-shifted maximum of R_4F_4 of 259 nm and an increase in negative ellipticity at the minimum at 281 nm for R_3F_3 and 284 nm for R_4F_4, which are due to the stacking of the four guanine rings present in dimers of c-di-GMP, showing that addition of the peptides stabilizes the homodimer.[33] The red shifting of peak positions for R_4F_4 is evidence of altered π-stacking in the complex between c-di-GMP and R_4F_4, which is not observed for the c-di-GMP complex with R_3F_3. TEM images for c-di-GMP with R_3F_3 show the formation of nanosheets (Figure S8c). In contrast, the TEM image for c-di-GMP with R_4F_4 shows the formation of a fibrous network structure (Figure S8e). Differences in structure also change the slope of the SAXS profiles in the low q region (Figure S8b,d), $I \sim q^{-n}$. The slope of the low q intensity for c-di-GMP alone is n = 0.8 consistent with locally extended structures. Upon addition of R_3F_3, the slope changes to n = 1.8 which suggests the formation of layered structures, such as bilayers as seen in the TEM images. The peptide alone has a SAXS profile with n = 3.5. For R_4F_4, the slope changes to n = 4.2, suggesting the presence of compact globular structures.

Congo red staining can be used to quantify the amount of polysaccharides produced by bacteria.[35] This has been used as an indirect measurement of c-di-GMP levels since these are correlated to polysaccharide expression.[35] Congo red binds to polysaccharides resulting in a decreased optical density (OD) when polysaccharide matrices are formed by the bacteria.[35] When adding R_4F_4 to *P. aeruginosa*, we observe a decrease in optical density of the supernatant (Figure 6c). This indicates enhanced biofilm growth, however, it was observed that, from 0.00613 to 0.025 wt %, there was a precipitate at the bottom of the tube, and some film growth occurred at the interface of the tube between the air and the solution (Figure 6d). *P. aeruginosa* is a motile organism, therefore is expected to form a biofilm at the interface.[36] At 0.05 wt % (0.5 mg/mL), a concentration that is the above the MIC in water and for which 37% biofilm viability is observed (Figure 6a), there is no biomass on the side of the tube, but there is a deposit on the bottom of the tube (Figure 6d). *P. aeruginosa* has a mucoidal phenotype, which means it can form a polysaccharide capsule around itself in response to stressed conditions.[37] Therefore, we conclude that the reduction in the OD is due to stressed bacteria producing polysaccharides as part of the stress response.

CONCLUSIONS

The two "blocky" surfactant-like peptides R_3F_3 and R_4F_4 are both able to self-assemble in aqueous solution at concentrations in excess of critical values, obtained from fluorescence probe assays. The cac = 0.3 wt % (≡ 3.2 mM) for R_3F_3 is higher than that previously obtained for the compositional homologue peptide RFRFRF, for which the cac = 2.3 mM.[16] On the other hand, the cac = 0.22 wt % (≡ 1.8 mM) for R_4F_4 is significantly higher than that previously reported for the compositional homologue RFRFRFRF, for which the cac = 0.34 mM.[16] This shows a significant influence of sequence on aggregation propensity. In addition, the nanostructure that self-assembles is distinct, since R_3F_3 forms a population of twisted nanotape structures whereas RFRFRF adopts a globular morphology. In the case of the longer peptides, nanosheets are formed by R_4F_4, whereas RFRFRFRF adopts a nanofiber morphology. The self-assembly of these peptides is likely driven by π-stacking interactions. This is supported by the observation in the CD spectra that the molar ellipticity of the 220 nm peak due to phenylalanine π-stacking increases from native pH to pH 7, as shown in Figures 1b and 2b.

The CD and FTIR spectra measured for R_3F_3 and R_4F_4 show that, even above the cac, these peptides do not adopt well-defined secondary structures, although there are π-stacking interactions. Furthermore, the SAXS intensity profiles suggest a significant component of unaggregated peptides in solution, also above the cac. Combined with the relatively high cac values (compared to typical surfactant-like peptides, such as A_9R[38] or lipidated peptides), this indicates that R_3F_3 and R_4F_4 have a weak aggregation propensity. This may be beneficial in terms of the observed antimicrobial activity, which is observed at concentrations an order of magnitude below the cac.

We found that both peptides have antimicrobial activity against *Pseudomonas* species, with R_4F_4 particularly active, killing all colony forming units of *P. aeruginosa* in planktonic form at 0.05 wt % (0.5 mg/mL). At this concentration, the cytotoxicity to human cells (fibroblast model) is relatively low. This peptide has a MIC of 0.045 wt % (0.45 mg/mL, 0.37 mM). This peptide also showed activity against other *Pseudomonas species*, in particular *P. syringae*, which is a widespread plant pathogen. We propose that the antimicrobial activity against *Pseudomonas* in planktonic form may be due to disruption of the bacterial lipid membrane, which contains ∼21% PG lipids and 60% PE lipids (the remainder being cardiolipin).[39,40] This 1:3 ratio of PG: PE corresponds to the composition where model vesicle membrane disruption is observed by SAXS and cryo-TEM (Figures 3 and 4) and this composition of vesicle has been used in prior studies of cationic antimicrobial peptide activity.[40]

We were then led to further examine the activity of lead candidate peptide R_4F_4 against *Pseudomonas* biofilms and a significant reduction in biofilm viability was observed through Crystal violet assays although biofilm formation was not completely inhibited. Since c-di-GMP is known to be an important signaling molecule involved in *Pseudomonas* biofilm formation, we then examined the interaction of the two peptides with this nucleotide. Circular dichroism confirmed an interaction with the peptides which stabilizes the homodimer form of c-di-GMP and in the case of R_4F_4, modification of π-

https://dx.doi.org/10.1021/acsabm.9b00894
ACS Appl. Bio Mater. XXXX, XXX, XXX−XXX

stacking interactions was observed. These observations point to a possible role of these arginine-rich peptides as binders of c-di-GMP, and this is a possible mechanism of biofilm inhibition. The arginine guanidinium group is known to bind c-di-GMP through electrostatic interactions and hydrogen bonding, and this was further probed using Congo red staining of polysaccharides, which were overexpressed by bacteria exposed to the antimicrobial activity of R_4F_4.

In summary, R_4F_4 is a promising candidate peptide with pronounced antimicrobial activity against *Pseudomonas* species. Although R_3F_3 has some activity against *Pseudomonas aeruginosa*, the increased molecular weight of R_4F_4 seems to confer higher activity. It would be expected that longer diblock peptides would potentially have higher antimicrobial activity, due to the increased cationic charge. However, this increased charge might result in increased toxicity to human cells, thus future work could focus on finding an optimum length of peptide with a balance of cytocompatibility, and antimicrobial activity. Peptide R_4F_4 is more active against *Pseudomonas* species than RA_6R and RA_9R studied in our previous work.[28] Also promising is the fact that the specific activity against *Pseudomonas* species is likely to slow antimicrobial resistance to the peptide because wide spectrum actives often develop resistance faster.

Further work could explore chemical modification to enhance the activity of R_4F_4 against biofilm formation and c-di-GMP binding capacity, along with other modifications, such as insertion of protecting groups/lipidation/use of D-amino acids or other non-natural residues, to enhance stability in vivo for potential future application.

MATERIALS AND METHODS

Materials. R_3F_3 and R_4F_4 were synthesized by Peptide Synthetics (Fareham, UK). Purity was determined by HPLC, and for R_3F_3 was found to be 97.83%, the molar mass from ESI-MS was M_w = 928.089 g mol^{-1}. The purity of R_4F_4 was 97.98%, and the molar mass from ESI-MS was M_w= 1231.452 g mol^{-1}.

Sample Preparation. Samples of R_3F_3 and R_4F_4 were dissolved in water. The native pH was found to be 2.22 and 2.28, respectively. Adjustment of pH to pH 7.0 was done using 0.5 M NaOH.

Fluorescence Assays. The critical aggregation concentrations (cac) of R_3F_3 and R_4F_4 were determined using fluorescence spectroscopy. Fluorescence spectra were recorded with a Varian Cary Eclipse fluorescence spectrometer with samples in 4 mm inner width quartz cuvettes. ANS (8-anilinonaphthalene-1-sulfonic acid) was used to probe the aggregation as a probe that is sensitive to hydrophobic environments making it suitable to locate the cac.[41] ANS assays were performed using a 66.8 μM ANS solution (1 mg of ANS dissolved in 50 mL water and sonicated for 30 min) to solubilize R_3F_3 and R_4F_4. Fluorescence spectra were recorded between 400 and 650 nm (λ_{ex}= 356 nm). Additionally, ThT was used to determine the cac of R_3F_3, as it is sensitive to the formation of amyloid fibrils at the cac.[42] ThT assays were performed using 5.0×10^{-3} wt % solution to solubilize the peptide. Spectra were recorded between 460 and 600 nm (λ_{ex}= 440 nm).

Circular Dichroism (CD). CD spectra were recorded using a Chirascan spectropolarimeter (Applied Photophysics, UK) in the wavelength range 180−260 nm (or 340 nm for samples with c-di-GMP). Samples 1 wt % of R_3F_3 and R_4F_4 in pure H_2O at native pH and pH 7 were pipetted into a quartz plate cell with 0.1 mm path length. Data with absorbance less than 2 only are reported. Measurements were recorded with a 0.5 nm bandwidth, 1 mm step and 1 s collection time per point. The CD signal for the background solution was subtracted from the CD signal of the sample, and molar ellipticity was calculated.

Fourier Transform Infrared Spectroscopy (FTIR). Spectra were recorded using a Thermo Scientific Nicolet iS5 instrument equipped with a DTGS detector, with a Specac Pearl liquid cell (sample contained between fixed CaF_2 plates). Aliquots 80 μL of 1 wt % R_3F_3 and R_4F_4 at native and pH 12 dissolved in D_2O were prepared and added into the liquid cell. Spectra were scanned 128 times over the range 900−4000 cm^{-1}

Transmission Electron Microscopy (TEM). Imaging was performed using a JEOL 2100Plus TEM microscope operated at 200 kV. Droplets of sample were placed on Cu grids coated with a carbon film (Agar Scientific, UK), stained with uranyl acetate (1 wt %) (Sigma-Aldrich, UK) and dried. Specimens were then loaded into the microscope.

Cryo-TEM. Vitrified specimens were prepared using an automated FEI Vitrobot device using Quantifoil 3.5/1 holey carbon copper grids with a hole size of 3.5 μm. Prior to use, grids were plasma cleaned using a Gatan Solarus 9500 plasma cleaner and then transferred into the environmental chamber of a FEI Vitrobot at room temperature and 100% humidity. Thereafter, sample solution was applied onto the grid, and it was blotted twice for 5 s and then vitrified in a 1/1 mixture of liquid ethane and propane at a temperature −180 °C. The grids with vitrified sample solution were maintained at liquid nitrogen temperature and then cryo-transferred to the microscope. Imaging was carried out using a field emission cryo-electron microscope (JEOL JEM-3200FSC) operating at 200 kV. Images were taken in bright field mode and using zero loss energy filtering (Ω type) with a slit width of 20 eV. Micrographs were recorded using a Gatan Ultrascan 4000 CCD camera. Specimen temperature was maintained at −187 °C during the imaging.

Liposome Preparation. Liposomes were prepared using the thin-layer hydration method. Weighed quantities of DPPG and DPPE were prepared by dissolution in chloroform, and thin lipid films were prepared by drying the lipids under a stream of nitrogen gas. Films were then placed under vacuum for 2 h to remove any remaining organic solvent. After this, lipids were resuspended in water to a final concentration of 0.5 wt % lipid, heated above their T_m and vortexed for 5 min. Liposome mixtures were then left to equilibrate before experiments. DPPG/DPPE vesicles were prepared using this method at different molar ratios of 1:3, 1:1, 3:1, and 1:0 DPPG/DPPE. To obtain peptide/lipid mixtures, resuspended lipids were added to peptide powders to make up a 0.08 wt % concentration of peptide, heated above the T_m and vortexed for 5 min, then left to equilibrate.

Small-Angle X-ray Scattering. Solution small-angle X-ray scattering (SAXS) data was collected on the bioSAXS beamline B21, at Diamond Light Source, Harwell, United Kingdom and beamline ID02 of the European Synchrotron Radiation Facility (ESRF), Grenoble France. On beamline B21, samples of 1 wt % R_3F_3 and 1 wt % R_4F_4 were loaded into PCR tubes in an automated sample changer. The samples were then delivered into a temperature-controlled quartz capillary and exposed for 1s, acquiring 30 frames at 20 °C. Data was collected using a Pilatus Dectris 2 M detector with a 3.9 m sample−detector distance and X-ray wavelength λ = 1.0 Å. Background was manually subtracted using ScÅtter. Form factor modeling was done using SASfit.

At ID02, samples were loaded into a glass capillary (internal radius = 2 mm) using a syringe. The beamline operated with an X-ray wavelength λ = 1.0 Å. 2D data was collected using a Rayonix MX170 detector, with a 1.474 m sample−detector distance.

Cell Viability Assays. The cytotoxicity of both R_3F_3 and R_4F_4 was examined. In vitro cell culture was conducted using 161Br (European Collection of Authenticated Cell Cultures, ECACC) cells, a human skin fibroblast cell line. Cells were cultured in EMEM (Eagle's minimum essential medium), with 2 mM glutamine, enriched with 15% fetal bovine serum (FBS) and 1% nonessential amino acids (NEAA). Cells were maintained in a humidified atmosphere of 37 °C, 5% CO_2.

Potential cytotoxicity effects were examined using the MTT (3-(4,5-dimethylthiazol-2-yl)-2,5-diphenyltetrazolium bromide) assay. The peptides were dissolved in complete media. Cells were seeded into a 96-well plate at 4×10^4 cells/mL and allowed to adhere for 24

https://dx.doi.org/10.1021/acsabm.9b00894
ACS Appl. Bio Mater. XXXX, XXX, XXX−XXX

h in 100 μL complete medium. After this, 100 μL of either complete media and/or peptide solution was added, to give either control solution, or solutions of peptide between the concentrations of 0.0625−4 mg/mL.

Cells were incubated for 67 h. After this, 20 μL MTT (5 mg/mL, in PBS) was added to each well plate and allowed to incubate for 5 h. After a further 5 h (72 h total), the solution was removed from the wells and replaced with 100 μL of DMSO per well, which dissolves the formazan crystals. Plates were incubated for 30 min, and then analyzed using a UV microplate reader (λ = 570 nm). Results are reported as a percentage cell viability compared to control (untreated) values, and fitted to a sigmoidal function using Origin Lab as a guide to the eye.

Antimicrobial Studies. The antimicrobial assays were performed with three types of bacteria which cause disease in humans, two being Gram-negative, *Escherichia coli* (K12) and *Pseudomonas aeruginosa* (PA01), and one being Gram-positive, *Staphylococcus aureus* (8325-4). Plant bacteria species *P. syringae*, *P. putida*, *P. agarici*, and *P. fluorcences* were also used to examine specificity against *Pseudomonas* species. Stock cultures were stored in −80 °C in 7% (v/v) DMSO. Prior to experiments, samples of all human bacteria were streaked out onto LB (Lysogeny Broth) agar and grown overnight at 37 °C, whereas the plant bacteria were grown overnight at 27 °C.

Bacterial Survival Assays. To examine whether the peptides were bactericidal, one colony from streaked plates was transferred into 7 mL of sterile lysogeny broth (LB), and grown overnight at 37 °C under agitation at 150 rev/min, on an orbital shaker, and these cultures were used for ongoing experiments. Cultures were then transferred into a 15 mL Falcon tube and cells were harvested by centrifugation at 9000 rpm at 4 °C for 10 min. The supernatant was discarded, and the pellet was resuspended in 1.5 mL of ice-chilled PBS (phosphate buffered saline).

After this, 30 μL of this solution was transferred into 300 μL of 0.5 mg/mL (or 0.05 wt %) of R_3F_3 or R_4F_4, in sterile water or control solutions of 300 μL of sterile water. Solutions were then vortexed for 5 s, and three 20 μL samples were taken at times 0, 120, and 1440 min. These samples were then serially diluted in PBS, and 10 μL of each dilution was platted onto LB agar and incubated at 37 °C overnight before colony counting.

Biofilm Assays. To form a biofilm, *Pseudomonas aeruginosa* PA01 and ATCC2363 strains were grown overnight in LB media. Following this, the culture was diluted 1:100 in M63 minimal medium supplemented with arginine and magnesium sulfate, with and without R_3F_3 or R_4F_4, with four technical replicates. After this the plate was incubated for 4−24 h.

Following incubation, the supernatant was discarded and then gently washed in water several times to decrease background staining. After this, 125 μL of 0.1 wt % crystal violet solution was added to each well of the microtiter plate and incubated for 10 min. Following this, the plate was washed several times and left to dry overnight.

Next, 125 μL of 30% acetic acid in water was added, to solubilize the biofilm, and the plate was incubated for further 10 min to allow solubilization. Absorbance was measured using a plate reader at 550 nm. Anova and Tukey were used to assess statistical significance.

Indirect Measurements of c-di-GMP Using Congo Red. *Pseudomonas aeruginosa* PA01 was grown overnight in LB media. After this, the culture was diluted 1:100 in 1 mL of M63 minimal medium supplemented with 0.4% L-arginine and 1 mM magnesium sulfate, with 40 μg/mL Congo red with and without R_4F_4.Control solutions were also prepared using the described medium above with no bacterial cells present. Congo red provides an indirect measure of c-di-GMP levels as it binds to the matrix of the biofilm, production of which is correlated to c-di-GMP levels.[35] Samples were shaken at 200 rpm overnight in a shaking incubator. After this, 200 μL of supernatant was added in triplicate to a 96 well place, and measured using a plate reader at 490 nm. Results are reported as (control solution OD − bacteria containing solution OD). Student's *t* tests were used to assess significance.

■ ASSOCIATED CONTENT

Supporting Information

The Supporting Information is available free of charge at https://pubs.acs.org/doi/10.1021/acsabm.9b00894.

SAXS fit parameters, TEM images, CD spectra of peptides with DPPG, cytotoxicity profiles, additional antimicrobial and biofilm activity assay results, and peptide binding with c-di-GMP data (PDF)

■ AUTHOR INFORMATION

Corresponding Author

Ian W. Hamley − *School of Chemistry, Pharmacy and Food Biosciences, University of Reading, Reading RG6 6AD, U.K.*; orcid.org/0000-0002-4549-0926; Email: I.W.Hamley@reading.ac.uk

Authors

Charlotte J. C. Edwards-Gayle − *School of Chemistry, Pharmacy and Food Biosciences, University of Reading, Reading RG6 6AD, U.K.*

Glyn Barrett − *School of Biological Sciences, University of Reading, Reading RG6 6AD, U.K.*

Shyamali Roy − *School of Biological Sciences, University of Reading, Reading RG6 6AD, U.K.*

Valeria Castelletto − *School of Chemistry, Pharmacy and Food Biosciences, University of Reading, Reading RG6 6AD, U.K.*; orcid.org/0000-0002-3705-0162

Jani Seitsonen − *Nanomicroscopy Center, Aalto University, FIN-02150 Espoo, Finland*

Janne Ruokolainen − *Nanomicroscopy Center, Aalto University, FIN-02150 Espoo, Finland*

Complete contact information is available at: https://pubs.acs.org/10.1021/acsabm.9b00894

Notes

The authors declare no competing financial interest.

■ ACKNOWLEDGMENTS

This work was supported by the award of a studentship to C.J.C. cofunded by the University of Reading and Diamond Light Source. Work of I.W.H. was supported by EPSRC Platform Grant ref EP/L020599/1. We are grateful to Diamond Light Source for beamtime on B21 (refs sm17118-1 and sm18523-1), Nathan Cowieson and Katsuaki Inoue for help, and ESRF for beamtime on ID02 (ref SC4739), and Alessandro Mariani for assistance.

■ REFERENCES

(1) Falla, T. J.; Karunaratne, D. N.; Hancock, R. E. W. Mode of Action of the Antimicrobial Peptide Indolicidin. *J. Biol. Chem.* **1996**, *271* (32), 19298−19303.

(2) Chan, D. I.; Prenner, E. J.; Vogel, H. J. Tryptophan- and Arginine-Rich Antimicrobial Peptides: Structures and Mechanisms of Action. *Biochim. Biophys. Acta, Biomembr.* **2006**, *1758* (9), 1184−1202.

(3) Brogden, K. A. Antimicrobial Peptides: Pore Formers or Metabolic Inhibitors in Bacteria? *Nat. Rev. Microbiol.* **2005**, *3* (3), 238−250.

(4) Tieleman, D. P. The Molecular Basis of Electroporation. *BMC Biochem.* **2004**, *5*, 10.

(5) Hamley, I. W. Small Bioactive Peptides for Biomaterials Design and Therapeutics. *Chem. Rev.* **2017**, *117* (24), 14015−14041.

(6) Schmidt, N.; Mishra, A.; Lai, G. H.; Wong, G. C. L. Arginine-Rich Cell-Penetrating Peptides. *FEBS Lett.* **2010**, *584* (9), 1806−1813.
(7) Hauser, C. A. E.; Zhang, S. Designer Self-Assembling Peptide Nanofiber Biological Materials. *Chem. Soc. Rev.* **2010**, *39* (8), 2780−2790.
(8) Hamley, I. W. Self-Assembly of Amphiphilic Peptides. *Soft Matter* **2011**, *7*, 4122−4138.
(9) Dehsorkhi, A.; Castelletto, V.; Hamley, I. W. Self-Assembling Amphiphilic Peptides. *J. Pept. Sci.* **2014**, *20* (7), 453−467.
(10) Chen, C.; Pan, F.; Zhang, S.; Hu, J.; Cao, M.; Wang, J.; Xu, H.; Zhao, X.; Lu, J. R. Antibacterial Activities of Short Designer Peptides: A Link between Propensity for Nanostructuring and Capacity for Membrane Destabilization. *Biomacromolecules* **2010**, *11* (2), 402−411.
(11) Dehsorkhi, A.; Castelletto, V.; Hamley, I. W.; Seitsonen, J.; Ruokolainen, J. Interaction between a Cationic Surfactant-like Peptide and Lipid Vesicles and Its Relationship to Antimicrobial Activity. *Langmuir* **2013**, *29* (46), 14246−14253.
(12) Hamley, I. W.; Dehsorkhi, A.; Castelletto, V. Self-Assembled Arginine-Coated Peptide Nanosheets in Water. *Chem. Commun.* **2013**, *49* (18), 1850−1852.
(13) Castelletto, V.; Barnes, R. H.; Karatzas, K. A.; Edwards-Gayle, C. J. C.; Greco, F.; Hamley, I. W.; Rambo, R.; Seitsonen, J.; Ruokolainen, J. Arginine-Containing Surfactant-Like Peptides: Interaction with Lipid Membranes and Antimicrobial Activity. *Biomacromolecules* **2018**, *19* (7), 2782−2794.
(14) Castelletto, V.; Barnes, R.; Karatzas, K.-A.; Edwards-Gayle, C. J. C.; Greco, F.; Hamley, I. W.; Seitsonen, J.; Ruokolainen, J. Restructuring of Lipid Membranes by an Arginine-Capped Peptide Bolaamphiphile. *Langmuir* **2019**, *35* (5), 1302−1311.
(15) Decandio, C. C.; Silva, E. R.; Hamley, I. W.; Castelletto, V.; Liberato, M. S.; Oliveira, V. X.; Oliveira, C. L. P.; Alves, W. A. Self-Assembly of a Designed Alternating Arginine/Phenylalanine Oligopeptide. *Langmuir* **2015**, *31* (15), 4513−4523.
(16) Silva, E. R.; Listik, E.; Han, S. W.; Alves, W. A.; Soares, B. M.; Reza, M.; Ruokolainen, J.; Hamley, I. W. Sequence Length Dependence in Arginine/Phenylalanine Oligopeptides: Implications for Self-Assembly and Cytotoxicity. *Biophys. Chem.* **2018**, *233*, 1−12.
(17) Slyngborg, M.; Nielsen, D. A.; Fojan, P. The Physical Properties and Self-Assembly Potential of the RFFFR Peptide. *ChemBioChem* **2016**, *17* (21), 2083−2092.
(18) Malanovic, N.; Leber, R.; Schmuck, M.; Kriechbaum, M.; Cordfunke, R. A.; Drijfhout, J. W.; de Breij, A.; Nibbering, P. H.; Kolb, D.; Lohner, K. Phospholipid-Driven Differences Determine the Action of the Synthetic Antimicrobial Peptide OP-145 on Gram-Positive Bacterial and Mammalian Membrane Model Systems. *Biochim. Biophys. Acta, Biomembr.* **2015**, *1848* (10), 2437−2447.
(19) Arouri, A.; Dathe, M.; Blume, A. Peptide Induced Demixing in PG/PE Lipid Mixtures: A Mechanism for the Specificity of Antimicrobial Peptides towards Bacterial Membranes. *Biochim. Biophys. Acta, Biomembr.* **2009**, *1788* (3), 650−659.
(20) Epand, R. M.; Rotem, S.; Mor, A.; Berno, B.; Epand, R. F. Bacterial Membranes as Predictors of Antimicrobial Potency. *J. Am. Chem. Soc.* **2008**, *130* (43), 14346−14352.
(21) Li, J.; Wang, X.; Zhang, T.; Wang, C.; Huang, Z.; Luo, X.; Deng, Y. A Review on Phospholipids and Their Main Applications in Drug Delivery Systems. *Asian J. Pharm. Sci.* **2015**, *10* (2), 81−89.
(22) Krysmann, M. J.; Castelletto, V.; Hamley, I. W. Fibrillisation of Hydrophobically Modified Amyloid Peptide Fragments in an Organic Solvent. *Soft Matter* **2007**, *3* (11), 1401−1406.
(23) Castelletto, V.; Hamley, I. W. Methods to Characterize the Nanostructure and Molecular Organization of Amphiphilic Peptide Assemblies. In *Peptide Self-Assembly: Methods and Protocols*; Nilsson, B. L., Doran, T. M., Eds.; Springer New York: New York, NY, 2018; pp 3−21. DOI: 10.1007/978-1-4939-7811-3_1.
(24) Barth, A. Infrared Spectroscopy of Proteins. *Biochim. Biophys. Acta, Bioenerg.* **2007**, *1767* (9), 1073−1101.
(25) Barth, A. The Infrared Absorption of Amino Acid Side Chains. *Prog. Biophys. Mol. Biol.* **2000**, *74* (2000), 141−173.
(26) Castelletto, V.; Gouveia, R. M.; Connon, C. J.; Hamley, I. W. New RGD-Peptide Amphiphile Mixtures Containing a Negatively Charged Diluent. *Faraday Discuss.* **2013**, *166*, 381−397.
(27) Breßler, I.; Kohlbrecher, J.; Thünemann, A. F. *SASfit*: A Tool for Small-Angle Scattering Data Analysis Using a Library of Analytical Expressions. *J. Appl. Crystallogr.* **2015**, *48* (5), 1587−1598.
(28) Creighton, T. E. *Proteins: Structures and Molecular Properties*; W.H. Freeman, 1992. DOI: 10.1016/0968-0004(85)90239-7.
(29) Edwards-Gayle, C. J. C.; Castelletto, V.; Hamley, I. W.; Barrett, G.; Greco, F.; Hermida-Merino, D.; Rambo, R. P.; Seitsonen, J.; Ruokolainen, J. Self-Assembly, Antimicrobial Activity, and Membrane Interactions of Arginine-Capped Peptide Bola-Amphiphiles. *ACS Appl. Bio Mater.* **2019**, *2* (5), 2208−2218.
(30) Hamley, I. W. *Introduction to Peptide Science*; Wiley: 2020, in press.
(31) Kulasekara, B. R.; Christen, M.; Miller, S. I.; Kulasekara, H. D.; Christen, B.; Hoffman, L. R. Asymmetrical Distribution of the Second Messenger c-di-GMP upon Bacterial Cell Division. *Science* **2010**, *328* (5983), 1295−1297.
(32) Jenal, U.; Reinders, A.; Lori, C. Cyclic Di-GMP: Second Messenger Extraordinaire. *Nat. Rev. Microbiol.* **2017**, *15* (5), 271−284.
(33) Foletti, C.; Kramer, R. A.; Mauser, H.; Jenal, U.; Bleicher, K. H.; Wennemers, H. Functionalized Proline-Rich Peptides Bind the Bacterial Second Messenger c-di-GMP. *Angew. Chem., Int. Ed.* **2018**, *57* (26), 7729−7733.
(34) Peeters, E.; Nelis, H. J.; Coenye, T. Comparison of Multiple Methods for Quantification of Microbial Biofilms Grown in Microtiter Plates. *J. Microbiol. Methods* **2008**, *72* (2), 157−165.
(35) Jones, C. J.; Wozniak, D. J. Congo Red Stain Identifies Matrix Overproduction and Is an Indirect Measurement for c-di-GMP in Many Species of Bacteria. In *c-Di-GMP Signaling. Methods in Molecular Biology*; Sauer, K., Ed.; Human Press, 2017.
(36) O'Toole, G. A. Microtiter Dish Biofilm Formation Assay. *J. Visualized Exp.* **2011**, No. 47, 10−11.
(37) Sabra, W.; Kim, E.-J.; Zeng, A.-P. Physiological Responses of Pseudomonas Aeruginosa PAO1 to Oxidative Stress in Controlled Microaerobic and Aerobic Cultures. *Microbiology* **2002**, *148* (10), 3195−3202.
(38) Castelletto, V.; Edwards-Gayle, C. J. C.; Hamley, I. W.; Barrett, G.; Seitsonen, J.; Ruokolainen, J. Peptide-Stabilized Emulsions and Gels from an Arginine-Rich Surfactant-Like Peptide with Antimicrobial Activity. *ACS Appl. Mater. Interfaces* **2019**, *11* (10), 9893−9903.
(39) Epand, R. F.; Savage, P. B.; Epand, R. M. Bacterial Lipid Composition and the Antimicrobial Efficacy of Cationic Steroid Compounds (Ceragenins). *Biochim. Biophys. Acta, Biomembr.* **2007**, *1768* (10), 2500−2509.
(40) Epand, R. M.; Epand, R. F. Bacterial Membrane Lipids in the Action of Antimicrobial Agents. *J. Pept. Sci.* **2011**, *17* (5), 298−305.
(41) Hawe, A.; Sutter, M.; Jiskoot, W. Extrinsic Fluorescent Dyes as Tools for Protein Characterization. *Pharm. Res.* **2008**, *25* (7), 1487−1499.
(42) LeVine, H. Quantification of β-Sheet Amyloid Fibril Structures with Thioflavin T. *Methods Enzymol.* **1999**, *309*, 274−284.

https://dx.doi.org/10.1021/acsabm.9b00894
ACS Appl. Bio Mater. XXXX, XXX, XXX−XXX